5 Total Internal Reflection Fluorescence Microscopy in Vascular Smooth Muscle

Madeline Nieves-Cintrón, Sendoa Tajada, L. Fernando Santana, and Manuel F. Navedo

CONTENTS

5.1 INTRODUCTION

Total internal reflection fluorescence (TIRF) is a microscopy technique that relies on the evanescent field generated when light waves are totally internally reflected at the coverslip-buffer interface.[1,2] This distinct illumination mode allows the selective excitation of fluorophores and subsequent visualization of fluorescence signals in a restricted region of a sample near the glass-media interface. The evanescent field generated has excitation qualities similar to the original light source and only excites fluorophores within ~100 nm of the coverslip. The limited penetration of the evanescent field decreases out-of-focus fluorescent signals, thus enabling the study of cellular events at membrane/submembrane regions with high signal-to-noise ratio. Indeed, a critical advantage of TIRF microscopy (TIRFM) over other microscopy approaches is its ability to acquire images of membrane/submembrane regions with high resolution and contrast. This has led to a flurry of studies that examine mechanisms mediating protein trafficking, and calcium (Ca^{2+}) signals in membrane/submembrane regions.[3–6]

The elemental second messenger Ca^{2+} plays an important role in diverse signaling processes in excitable cells, including vascular smooth muscle. It is increasingly recognized that spatial and temporal regulation of Ca^{2+} signals provides the means for controlling signaling specificity and excitability in vascular smooth muscle.[7] Indeed, the proper integration of multiple Ca^{2+} signaling events that influence intracellular Ca^{2+} ($[Ca^{2+}]_i$) in vascular smooth muscle is required to arrive at the appropriate physiological response. This is achieved through steep Ca^{2+} ion gradients, which are maintained between the cytosol and the extracellular milieu, as well as intracellular organelles through active transport. Different classes of Ca^{2+}-permeable channels at the plasma membrane and sarcoplasmic reticulum (SR) contribute to the movement of Ca^{2+} ions down their gradient, thus affecting changes in intracellular Ca^{2+} and further fine-tuning Ca^{2+} signal specificity and cell excitability.[7] Whereas Ca^{2+} signals produced by Ca^{2+}-permeable channels located in the SR have been extensively examined using confocal and/or epifluorescence microscopy, those mediated by Ca^{2+}-permeable channels at the plasma membrane are less understood due to technical limitations with these techniques. The development of faster and brighter Ca^{2+} indicators, together with the advent of TIRFM, has facilitated the study of plasmalemmal Ca^{2+}-permeable channels and their contribution to Ca^{2+} signals and cellular function.

The Ca^{2+} signals produced by the opening of plasmalemmal Ca^{2+}-permeable channels are known as *sparklets*. In this chapter, we provide an overview of the basic concepts behind TIRFM, and its application to the study of the function and regulation of plasmalemmal Ca^{2+}-permeable channels in vascular smooth muscle. This approach could be easily applicable to the study of Ca^{2+}-permeable channels in other cells.

5.2 TOTAL INTERNAL REFLECTION FLUORESCENCE MICROSCOPY

In this section, key aspects of TIRFM are summarized, but more in-depth reviews about the physics behind TIRFM can be found in the published literature.[1,2,6] TIRFM utilizes an evanescent wave to selectively excite fluorophores in regions of a sample directly adjacent to the glass coverslip-buffer interface (e.g., plasma membrane of

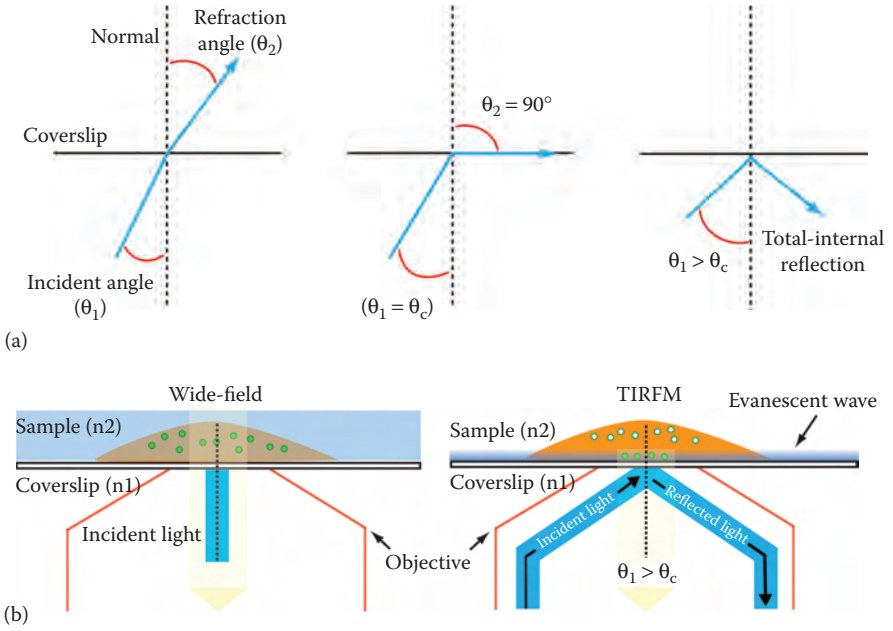

FIGURE 5.1 Diagram of a basic TIRFM system. (a) Schematic representation of the bending of incident light as it propagates through medium of different refractive indexes and (b) diagrams of specimen illumination in wide-field and TIRFM. Please see text for details.

adherent cells) (Figure 5.1). Such arrangement allows for unparalleled signal-to-noise ratio, where one can visualize the fluorophores located in the near-membrane space, with little noise being emitted from fluorophores in other parts of the cell. The principles at the heart of TIRFM are based on the laws of refraction of light and properties of the refractive media.[2] The refractive index (n) of a material describes how light propagates through that material compared to how it will travel in a vacuum. It is defined as $n = c/v$, where c is the speed of light in a vacuum and v is the velocity of light in the material. When light travels through mediums of different refractive indexes, the light rays will bend in function of the angle of incidence in accordance to Snell's law:

$$n_1 \sin\theta_1 = n_2 \sin\theta_2$$

where:

- n_1 is the medium with higher refractive index
- n_2 is the lower refractive index medium
- θ_1 is the angle of incidence with respect to the normal
- θ_2 is the angle of refracted light at the interface into the medium of lower refractive index

For example, vascular smooth muscle cells in aqueous media are allowed to adhere to the glass coverslip, which represents the media of high refractive index (n_1), whereas the

aqueous buffer is the media with lower refractive index (n_2). The angle of incidence determines the angle of refraction (i.e., if the angle of incidence increases, so does the angle of refraction). When the angle of incidence θ_1 reaches a critical value θ_c (i.e., $\theta_1 = \theta_c$), the refraction angle $\theta_2 = 90°$ degrees, and the refracted light travels along the surface of the coverslip. According to Snell's law, the critical angle θ_c is given by

$$\theta_c = \sin^{-1}\left(\frac{n_2}{n_1}\right)$$

When the angle of incidence is greater than the critical angle, light is no longer refracted, but totally reflected (Figure 5.1a). The transition from refraction to reflection is a continuous process in which light goes from predominantly refracted with minimal reflection to total internal reflection back into the coverslip when the angle of incidence exceeds the critical angle. This phenomenon of total internal reflection leads to the generation of an electromagnetic field at the interface, which is known as the evanescent wave or evanescent field. This evanescent wave has excitation properties similar to those of the light source (Figure 5.1b). The evanescent wave propagates along the surface and its intensity decays exponentially with increasing distance from the interface, as described by the following equation:

$$I_z = I_0 \exp\left(\frac{-Z}{d}\right)$$

where:

I_z is the intensity at a perpendicular distance z from the interface
I_0 is the intensity of the evanescent field at the interface (i.e., $z = 0$)
d is the penetration depth

The penetration depth is the perpendicular distance from the interface at which the excitation intensity is 1/e of I_0. In other words, it is the distance at which the intensity of the evanescent field excitation decays 37% of its intensity at the interface. (In depth discussion of I_0 and how it relates to the incident beam angle and polarization are described elsewhere[1,2]). The wavelength (λ) of the excitation light, incidence angle of excitation (θ), and the refractive indices of the glass coverslip and the sample (n_1 and n_2, respectively) determine the penetration depth according to the following equation:

$$d = \frac{\lambda_0}{4\pi\sqrt{n_1^2 \sin\theta - n_2^2}}$$

Therefore, a lower penetration depth can be achieved with larger angles of incidence. In most TIRFM systems, the evanescent wave extends ~70–200 nm into the sample. This characteristic of the evanescent wave is the key to the axial resolution achieved with TIRFM (Figure 5.1). In practice, the penetration depth can be adjusted by changing the angle of incidence, since the excitation wavelength is usually limited by available fluorophores, and the refractive indices of the cell are out of the

investigator's control. This is an important consideration when setting up a TIRFM system, particularly an objective-based system, since the objective numerical aperture (NA) directly influences the angles of incidence (see below).

TIRFM relies on the ability to introduce light at angles exceeding a critical angle. Initially, the required angle of illumination was achieved by using a prism to direct excitation light to the appropriate angle of incidence. Prism-based TIRFM has many advantages, including the cost effectiveness, generation of a purer evanescent wave due to minimal scattering of light and ease of customization. A drawback, however, is that it requires the glass coverslip to be optically coupled to the prism using liquid substances like glycerol, which complicates the set-up of each experiment and limits the potential use in high throughput applications. In addition, positioning of the prism in some configurations may limit access to the specimen, thus rendering manipulations cumbersome. This is an important consideration for studies using TIRFM to examine ion channel function, as it is recommended that TIRFM be applied in combination with whole-cell patch clamp (see Section 5.3.2).[8]

Objective-based TIRFM, in which excitation light is delivered through the objective, is also available. An advantage of objective-based TIRFM is that it does not require optical coupling between the coverslip and the prism, so it is easier to use. Other advantages include the ability to easily change angle of incidence and wavelength. Achieving angles larger than the critical angle requires an objective with high NA. The NA of the objective limits the range of possible angles of incidence. The minimal NA necessary for TIRFM is 1.4, but higher values (1.45–1.49) are desirable since they allow broader ranges of illumination angles and hence penetration depths.[6]

5.3 MEASURING Ca^{2+}-PERMEABLE CHANNEL ACTIVITY IN THE PLASMA MEMBRANE OF VASCULAR SMOOTH MUSCLE CELLS WITH TOTAL INTERNAL REFLECTION FLUORESCENCE MICROSCOPY

A particular innovative use of TIRFM has been on the recording of Ca^{2+} signals produced by the opening of Ca^{2+}-permeable channels at the plasma membrane of a cell, including vascular smooth muscle cells.[4,9–15] These Ca^{2+} signals are known as Ca^{2+} sparklets, a term first coined to define Ca^{2+} influx produced by the opening of voltage-gated Ca^{2+} channels in cardiac cells.[16] Since then, optical recording of Ca^{2+} influx produced by other Ca^{2+}-permeable channels and pores has been described, thus making the use of the term sparklet generic.[4,9–13,17–22] To remove ambiguity, the term *sparklet* is usually preceded by the name of the underlying channel (e.g., L-type $Ca_V1.2$ sparklet).

The optical recording of Ca^{2+} influx through Ca^{2+}-permeable channels is important because our ability to visualize micro and/or nanodomain Ca^{2+} signals at the plasma membrane in space and time is essential for fully understanding cell function under physiological and pathological conditions. The biophysical properties of Ca^{2+}-permeable channels at the plasma membrane of any cell have

been mainly examined using the patch-clamp technique. Although powerful, this approach has some limitations in that it doesn't provide information about the localization and/or organization of functional Ca^{2+}-permeable channels. The combined use of patch-clamp with TIRFM has helped overcome these limitations and has revealed new features associated with channel activity and gating modality, which has improved our understanding of the function of plasmalemmal Ca^{2+}-permeable channels. Much of this new information has been obtained by optically recording the activity of plasmalemmal Ca^{2+}-permeable channels with TIRFM in vascular smooth muscle cells.[8,12,14,15] In this section we describe a protocol for isolation of vascular smooth muscle cells, which is critical for acquisition of high quality data, and technical details related to the use of TIRFM to study submembrane Ca^{2+} signals in these cells.

5.3.1 Vascular Smooth Muscle Cell Isolation

The quality of vascular smooth muscle cells is critical for successful recording of sparklets using TIRFM. Single vascular smooth muscle cells can be obtained by enzymatic digestion of freshly dissected arteries from different vascular beds. Dissociation protocols are provided for two well-established preparations: cerebral arteries and mesenteric arteries (third and fourth order). For cerebral vascular smooth muscle isolation, arteries are dissected at 4°C in magnesium physiological saline solution (Mg^{2+}PSS) buffer composed of (in mM): 140 NaCl, 5 KCl, 2 $MgCl_2$, 10 D-glucose, and 10 HEPES, pH 7.4 with NaOH. Clusters of arteries, which are floating freely and ideally settled at the bottom of a Wheaton V-vial, are digested in Mg^{2+}PSS buffer supplemented with papain (1 mg/mL; Worthington LS003119) and dithiothreitol (1 mg/mL; Sigma D9163) in a water bath at 37°C for 7 minutes, then incubated in Mg^{2+}PSS buffer supplemented with collagenase type H (0.3 mg/mL; Sigma C8051) and collagenase type F (0.7 mg/mL; Sigma C7926) at 37°C for 7 minutes. For mesenteric vascular smooth muscle cells isolation, clusters of freely floating arteries that settled at the bottom of a Wheaton V-vial are incubated in Mg^{2+}PSS buffer supplemented with papain (1 mg/mL) and dithiothreitol (1 mg/mL) in a water bath at 37°C for 10 minutes. After 10 minutes, the papain enzyme mix is taken out and replaced with Mg^{2+}PSS buffer supplemented with 1.77 mg ml collagenase type H (Sigma; C8051), Elastase (0.5 mg/ml; Worthington LS002292), and 1 mg/ml Soybean Trypsin Inhibitor (1 mg/ml; Sigma T9003). Immediately after the enzyme solution is removed, arteries are washed three times in ice-cold Mg^{2+}PSS buffer, being careful to not disturb the cluster of vessels. After the last wash, arteries are allowed to rest in ice-cold Mg^{2+}PSS buffer for 30 minutes before smooth muscle dissociation. In our experience, clusters of arteries that remain floating closer to the air-solution interface yield poor-quality cells after dissociation. Glass pipettes of decreasing diameters are used to triturate arteries to obtain single vascular smooth muscle cells by gently pipetting the digested arteries in solution up and down. Isolated cells are maintained in ice-cold Mg^{2+}PSS buffer until used. Figure 5.2 shows examples of high-quality and poor-quality cells for recording of sparklets using TIRFM.

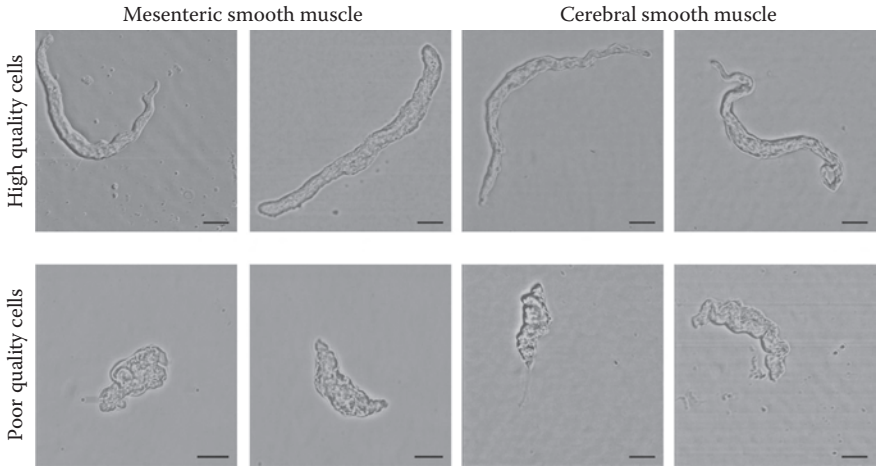

FIGURE 5.2 DIC image showing high quality (upper panels) or poor quality (lower panels) freshly dissociated mouse mesenteric and cerebral vascular smooth muscle cells for sparklet experiments using TIRFM. High quality smooth muscle cells exhibit relaxed, spindle-shaped and smoothed morphology, and attach very well to the coverslip. The resultant footprint of the TIRFM image may vary from that observed in the DIC as it is determined by cell area within the evanescent wave field. Poor quality cells are opaque and have a (semi-) contracted morphology that may be due to over digestion during the dissociation process. Scale bars = 10 μm.

5.3.2 Optical Recording of Plasmalemmal Ca^{2+}-Permeable Channels in Vascular Smooth Muscle Using Total Internal Reflection Fluorescence Microscopy

TIRFM, in combination with patch clamp electrophysiology, has been employed to optically record the activity of several plasmalemmal Ca^{2+}-permeable channels, including L-type $Ca_V1.2$ channels and transient receptor potential vanilloid 4 (TRPV4) channels, in vascular smooth muscle cells (Figure 5.3).[12,13] TIRFM has also been used to optically record TRPV4 channel activity in airway smooth muscle cells and L-type Ca^{2+} channel activity in smooth muscle from urinary bladder and portal veins.[20,23,24]

In a typical experiment, isolated smooth muscle cells are allowed to attach to a glass coverslip of a perfusion chamber mounted on an inverted microscope coupled to a TIRF module. After cell adhesion, cells are washed by continuous superfusion and patched in the whole-cell patch-clamp configuration. This accomplishes two main objectives: (1) control of membrane potential, which facilitates manipulation of the open probability of a channel and the driving force for Ca^{2+} influx, and (2) a conduit for delivery of substances (e.g., indicators, peptides, non-fluorescent Ca^{2+} buffers) through the patch pipette and into the cell. To eliminate Ca^{2+} release from the SR and prevent contamination of plasmalemmal Ca^{2+} signals with those produced by Ca^{2+} release from intracellular stores (e.g., Ca^{2+} sparks), cells are kept in physiological saline solution supplemented with the sarco/endoplasmic reticulum Ca^{2+}-ATPase (SERCA) inhibitor thapsigargin (1 μM), which prevents SR loading.

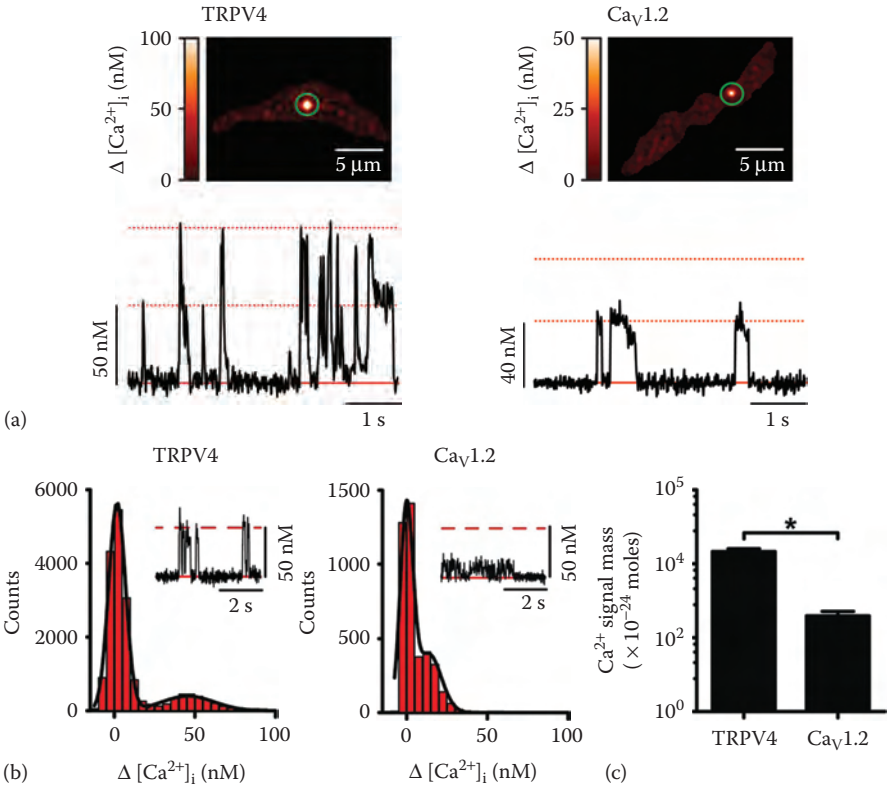

FIGURE 5.3 Examples of L-type $Ca_V1.2$ and TRPV4 sparklets in vascular smooth muscle. (a) TIRFM images of TRPV4 and L-type $Ca_V1.2$ sparklets recorded from freshly isolated vascular smooth muscle. TRPV4 sparklets were recorded with 2 mM extracellular Ca^{2+}, whereas L-type $Ca_V1.2$ sparklets were recorded with 20 mM extracellular Ca^{2+} in order to increase the driving force for Ca^{2+} and the amplitude of the quantal event. The traces below each image show the time-course of $[Ca^{2+}]_i$ in the site highlighted by the green circle in the images. Dotted lines represent the quantal level. (b) The amplitude of the signal mass of quantal TRPV4 and L-type $Ca_V1.2$ sparklets under physiological extracellular Ca^{2+} conditions. The insets show representative TRPV4 and L-type $Ca_V1.2$ sparklet recordings obtained with 2 mM extracellular Ca^{2+}. The solid line represents basal $[Ca^{2+}]_i$, whereas the dotted line marks the amplitude of quantal TRPV4 sparklets. Note that the quantal amplitude of L-type $Ca_V1.2$ sparklets significantly smaller than that of TRPV4 sparklets with 2 mM extracellular Ca^{2+}. The all-points histograms were generated from TRPV4 and L-type $Ca_V1.2$ sparklets recorded from vascular smooth muscle. The solid lines on the histograms represent best fits to data for TRPV4 ($q = 48$ nM) and L-type $Ca_V1.2$ ($q = 18$ nM) sparklets, and (c) the bar plot reveals that the signal mass of TRPV4 sparklets is larger than that of L-type $Ca_V1.2$ sparklets under similar experimental conditions. (Adapted from Mercado, J. et al., *J. Gen. Physiol.*, 143, 559–575, 2014. With permission.)

Once the whole-cell configuration is established, cells are loaded through the patch pipette with a fluorescent Ca^{2+} indicator, such as Fluo-5F (200 μM) and an excess of a non-fluorescent Ca^{2+} buffer, like EGTA (10 mM). Fluorescent indicators such as Fluo-5F are relatively fast binding Ca^{2+} dyes, whereas EGTA binds Ca^{2+} at a slower rate. The objective of this combination of indicator and EGTA is to facilitate that the faster Ca^{2+} indicator binds to Ca^{2+} first, thus producing a fluorescent signal. The duration of this signal will be limited as the slower but high affinity Ca^{2+} chelator EGTA buffers Ca^{2+} away. This maneuver will restrict the fluorescent signal to the Ca^{2+} entry site.[25] Images are acquired using through-the-lens TIRFM built around an inverted microscope equipped with 60x oil-immersion lens with appropriate NA (numerical aperture = 1.45), as described earlier. The microscope should be coupled to an ultra-fast (e.g., 100–500 Hz), highly sensitive (e.g., >90% quantum efficiency) electron multiplying charged-coupled device (EMCCD) camera, which is capable of detecting photons emitted from a single fluorescent molecule and recording two-dimensional images of dim fluorescent events at high speed. The use of this type of camera facilitates the recording of small, rare Ca^{2+} signal events, as well as allowing the imaging of relatively large areas of the cell. The very thin optical section afforded by the evanescent field during TIRFM (Figure 5.1b) extends ~100 nM from the surface of the coverslip, hence allowing the recording of small Ca^{2+} signals (e.g., sparklets) from submembrane regions, which are produced by the opening of Ca^{2+}-permeable channels, with high signal-to-noise ratio and adequate temporal resolution (Figure 5.3 for e.g., L-type $Ca_V1.2$ and TRPV4 sparklets).

5.4 SPARKLET ANALYSIS

To rigorously detect and analyze Ca^{2+} sparklet events, several automatic detection algorithms have been developed.[13,26,27] These algorithms facilitate analysis and prevent biases. An example of such an algorithm, developed by the Santana group, is the detection of Ca^{2+} signals as sparklets based on amplitude, and spatial and temporal criteria.[8,13,26] To be considered a sparklet, an elevation in Ca^{2+} needs to have an amplitude equal to or greater than the mean basal $[Ca^{2+}]_i$ plus three times its standard deviation. A sparklet site is then defined by a grid of 3×3 continuous pixels with $[Ca^{2+}]_i$ values at or above the amplitude threshold. Fluorescence signals can then be converted to concentration units to analyze sparklet events (after background subtraction) using the F_{max} equation as described by Maravall:

$$[Ca^{2+}] = K_d \frac{F/F_{max} - 1/R_f}{1 - F/F_{max}}$$

where:

F is the fluorescence
F_{max} is the indicator fluorescence intensity in the presence of saturating Ca^{2+} concentrations
K_d is the indicator dissociation constant
R is the indicator F_{max}/F_{min}
F_{min} is the fluorescence intensity of the indicator in Ca^{2+} free solution

K_d and R_f are properties of the indicator and, as such, are not influenced by factors that may vary among cells like resting [Ca^{2+}], for example. F_{max} should be obtained at the end of each experiment by exposing the cells to 20 mM Ca^{2+} external solution supplemented with the Ca^{2+} ionophore ionomycin (10 μM). This approach facilitates calibration of fluorescence signals within and between cells, which is critical for comparison during different experimental conditions.

After the signal is transformed to [Ca^{2+}] units, and given that the time course of Ca^{2+} sparklet events is comparable to that of single-channel current recordings, open probability analysis analogous to that used for single-channel currents can be applied to determine sparklet activity.[28] Thus, Ca^{2+} sparklet activity can be expressed as *nPs* for each sparklet site, where *n* is the number of quantal levels, and *Ps* is the probability that a Ca^{2+} sparklet site is active. Amplitude histograms can also be generated from these data and fitted with a Gaussian function such that the quantal nature of the signal can be revealed, if any. Poisson distribution analysis can also be implemented to assess the randomness of the spatial distribution of Ca^{2+} sparklet sites.

5.5 DIVERSE Ca^{2+} SPARKLET EVENTS IN VASCULAR SMOOTH MUSCLE

The most extensive characterization of sparklet events in vascular smooth muscle has been performed for L-type $Ca_V1.2$ sparklets and TRPV4 sparklets.[12,13,26] L-type $Ca_V1.2$ channels and TRPV4 channels play important roles in smooth muscle contraction and relaxation pathways, respectively.[29,30] The identification of L-type $Ca_V1.2$ channels and TRPV4 channels as the molecular entities underlying L-type $Ca_V1.2$ sparklets and TRPV4 sparklets, respectively, is based on multiple pharmacological, biophysical and molecular biology criteria for each channel.[12,13,26] For instance, L-type $Ca_V1.2$ sparklets can be activated by the L-type Ca^{2+} channel agonist Bay-K 8644 and inhibited by the L-type Ca^{2+} channel antagonist nifedipine, whereas TRPV4 sparklets are activated by the specific TRPV4 agonist GSK1016790A and are inhibited by the specific TRPV4 inhibitor HC-067047, but not by nifedipine.[12,13,26] It is worth noting that additional highly potent and very selective TRPV4 inhibitors are now available (e.g., GSK293874). Importantly, simultaneous recording of Ca^{2+} signals and underlying currents indicate that L-type $Ca_V1.2$ sparklets and TRPV4 sparklets are associated with an inward current with appropriate biophysical properties for each particular channel.[12,13,26] Furthermore, sparklets in tsA-201 cells expressing L-type $Ca_V1.2$ channels or TRPV4 channels reproduce all the basic features of native L-type $Ca_V1.2$ sparklets or TRPV4 sparklets, respectively.[12,13,26] This rigorous characterization should be extended to the study of sparklet events produced by any other plasmalemmal Ca^{2+}-permeable channel when using TIRFM.

L-type $Ca_V1.2$ and/or TRPV4 sparklets may influence $[Ca^{2+}]_i$, which may have important implications for vascular smooth muscle excitability. The contribution of sparklet events to $[Ca^{2+}]_i$ can be defined by the *signal mass* method developed by Zou and colleagues.[12,28,31] For this analysis, simultaneous electrical and optical recording of events is recommended. Total fluorescence (F_{total}) produced by a sparklet event is obtained from raw images by summing the indicator-associated fluorescence from

all the pixels in an area of the image sufficiently large as to encompass the entire fluorescence signal produced by a sparklet site. To determine the change in fluorescence (ΔF_{total}), the total fluorescence before the channel open is subtracted from the fluorescence at each time point during an opening. The signal mass is calculated by determining the peak of the integral of ΔF_{total} trace over time ($\int \Delta F_{total} dt$) for each Ca^{2+} sparklet. The charge influx (ΔQ) can be obtained by integrating the Ca^{2+}current underlying each sparklet. The signal mass of a Ca^{2+} sparklet and ΔQ have a linear relationship,[12,28] and the slope of this correlation can be used to convert Ca^{2+} sparklet signal mass into ΔQ values. The ΔQ values can then be used to provide an estimate of the potential impact of Ca^{2+} sparklets on $[Ca^{2+}]_i$ using the following equation:

$$\Delta[Ca^{2+}]_i = \frac{\Delta Q_{Ca}}{2FVBC}$$

where:

ΔQ_{Ca} is the change in Ca^{2+} influx (as calculated from signal mass analysis)
F is the Faraday constant
V refers to the accessible cytosolic volume
BC is the buffering capacity of the cell

Using this approach, L-type $Ca_V1.2$ sparklets were found to have an impact on local and global $[Ca^{2+}]_i$.[28] Interestingly, the signal mass of TRPV4 sparklets is ~100 times larger than that for L-type $Ca_V1.2$ sparklets, suggesting that total Ca^{2+} flux is higher through TRPV4 channels than L-type $Ca_V1.2$ channels in vascular smooth muscle (Figure 5.3b).[12] Considering the strong link between an increase in $[Ca^{2+}]_i$ and vascular smooth muscle contraction, it is thus remarkable that TRPV4 channel activity is associated with relaxation pathways.[30] Note, however, that the frequency of TRPV4 sparklet events is significantly lower compared to that of L-type $Ca_V1.2$ sparklets, thus allowing L-type $Ca_V1.2$ channels to conceivably contribute to global changes in $[Ca^{2+}]_i$.[12] Furthermore, the higher Ca^{2+} flux through TRPV4 channels may strengthen the functional coupling between these channels and its intended target (i.e., ryanodine receptors in the SR leading to activation of BK_{Ca} channels) to contribute to relaxation of vascular smooth muscle.[12,30] These observations highlight the complex nature of local Ca^{2+} signals in modulating global $[Ca^{2+}]_i$ and vascular smooth muscle excitability.[32]

5.6 UNIQUE FEATURES OF Ca^{2+} SPARKLETS IN VASCULAR SMOOTH MUSCLE REVEALED BY TOTAL INTERNAL REFLECTION FLUORESCENCE MICROSCOPY

The ability to optically record submembrane Ca^{2+} signals (i.e., sparklets) produced by the opening of plasmalemmal Ca^{2+}-permeable channels that are critical for vascular smooth muscle excitability using TIRFM has revealed important features regarding the differences in gating modality, and distinct regulation of activity and spatial organization of functional channels.[8,14,15]

5.6.1 Heterogeneous Sparklet Activity

The first major finding revealed by TIRFM is that both L-type $Ca_V1.2$ sparklets and TRPV4 sparklet sites are restricted to particular membrane regions.[12,13,26] These results are particularly striking considering the broad expression of L-type $Ca_V1.2$ channels and TRPV4 channels throughout the plasmalemma of vascular smooth muscle cells, as well as the stochastic nature of the channels' activity.[12,13,33,34] Indeed, Poisson analysis suggests that the spatial distribution of both L-type $Ca_V1.2$ sparklets and TRPV4 sparklet sites is non-stochastic, being higher at specific sites within the plasmalemma of vascular smooth muscle cells.[12,13] In addition, it was found that some L-type $Ca_V1.2$ sparklets showed stochastic and sporadic activity, whereas other sites have nearly continuous Ca^{2+} influx (e.g., persistent L-type $Ca_V1.2$ sparklets), thus suggesting that their activity is heterogeneous.[13,17,26] Multiple approaches have been used to determine the mechanisms responsible for regional variation in persistent Ca^{2+} sparklet activity in vascular smooth muscle. Extensive reviews on the subject can be found elsewhere.[8,14,15] Briefly, a working model has been proposed in which heterogeneous L-type $Ca_V1.2$ channel activity is determined by regional activity of protein kinases and phosphatases acting on neighboring channels to modulate their gating properties.[13,17,26,35,36] The scaffolding protein A kinase anchoring protein 150 (AKAP150) facilitates the formation of these functional units by bringing together protein kinases and phosphatases to the vicinity of the L-type $Ca_V1.2$ channel.[35–38] This local control model has profound functional implications considering that a surge in the frequency of persistent L-type $Ca_V1.2$ sparklets may result in an increase in Ca^{2+} influx, leading to vascular smooth muscle contraction. Indeed, persistent L-type $Ca_V1.2$ sparklet activity is increased in vascular smooth muscle during angiotensin II-induced hypertension and in animal models of diabetes via mechanisms that engage distinct kinase signaling pathways.[35,36,39] A similar AKAP150-driven arrangement has been found for TRPV4 channels in vascular smooth muscle, but its relevance during pathological conditions remains to be elucidated.[12]

5.6.2 Coupled Gating of Ion Channels in Vascular Smooth Muscle

Another unique feature revealed by TIRFM is that small clusters of L-type $Ca_V1.2$ and TRPV4 channels in vascular smooth muscle can open and close in unison (e.g., coupled gating).[12,37,40,41] Consistent with this coupled gating model, closer examination of the amplitude distribution of L-type $Ca_V1.2$ sparklets and TRPV4 sparklets, as well as the respective underlying Ca^{2+} currents, has demonstrated that the frequency of multichannel openings exceeds the probability of simultaneous openings of independently gated channels. A complementary approach to study coupled events is by quantifying coupling behavior based on a Markov chain model.[42] This model can be applied to Ca^{2+} sparklet and/or Ca^{2+} current traces to yield a coupling coefficient or coupling strength of a particular site. In this model, the activity of an ion channel can be modeled as a first-order, discrete Markov chain, and the transition matrix can be estimated from the sparklet and/or current records and their corresponding channel opening time courses using a built-in

Hidden Markov parameter estimation function. The estimated probability matrix can be modeled as a partially coupled Markov chain with three free parameters: κ is the coupling coefficient (or coupling strength) and ρ and ζ are the channel open-to-open and close-to-close probabilities, respectively. The value of κ can range from 0 for channels gating independently to 1 for channels exhibiting complete synchronization of openings. Implementation of this analysis has confirmed that while the majority of sparklet events produced by L-type $Ca_V1.2$ channels and TRPV4 channels result from the independent gating of channels, there is a subpopulation of channels that can undergo coupled gating.[37,40,41,43]

Coupled gating of Ca^{2+}-permeable channels, such as L-type $Ca_V1.2$ channels and TRPV4 channels, has important implications for Ca^{2+} signaling in vascular smooth muscle. Indeed, this gating modality may result in Ca^{2+} signaling amplification by oligomerization of Ca^{2+}-permeable channels, which may contribute to regulate vascular smooth muscle excitability. Consistent with this, the frequency of L-type $Ca_V1.2$ channels with coupled events is significantly elevated in vascular smooth muscle during hypertension and in diabetes, which could enhance arterial tone during these pathological conditions.[35,37] Representative TRPV4 coupled events can be observed in Figure 5.3a. The identification of coupled events within Ca^{2+} sparklets exemplifies the usefulness of complementary approaches (e.g., optics, electrophysiology, mathematical modeling) in creating a better comprehensive picture of physiological and pathological phenomena.

5.7 ADDITIONAL APPLICATIONS OF TOTAL INTERNAL REFLECTION FLUORESCENCE MICROSCOPY IN VASCULAR SMOOTH MUSCLE

Because of its intrinsic properties, TIRFM has been extensively used to visualize submembrane protein trafficking in living cells, including vascular smooth muscle. This application requires tagging of the protein of interest with a fluorescent tag, such as the enhanced green fluorescent protein (eGFP), and subsequent expression of the construct of interest in the desired cells (e.g., vascular smooth muscle). Cells are allowed to settle and attach to the coverslip, after which, images are collected using the TIRFM with appropriate laser excitation before and after a stimulus. Subsequently, fluorescent intensity is measured in each frame and plotted against time. Using a comparable approach, it was found that dynamic membrane trafficking of the transient receptor potential melastatin 4 (TRPM4) channel in vascular smooth muscle cells contributed to vascular reactivity through a mechanism that requires protein kinase C (PKC) δ activity.[44] Another study found that in cultured A7r5 cells, hydrogen peroxide stimulated the trafficking of transient receptor potential canonical 6 (TRPC6) channels.[45] However, care should be taken with interpretation of these results and their extrapolation to effects on vascular reactivity, as many of these experiments are typically performed in cultured, non-contractile cells due to technical limitations of transfection/infection of native cells. Thus, these trafficking experiments should be complemented with additional approaches, such as surface biotinylation assay using native vascular smooth muscle.[46]

The Amberg Group developed another application that employs the TIRFM technique for the simultaneous recording of L-type $Ca_V1.2$ sparklets and the generation of endogenous reactive oxygen species (ROS).[47] Using the ROS indicator DCF and the Ca^{2+} indicator fluo 5F, this group demonstrated that the generation of ROS puncta localize and preceded the activation of persistent L-type $Ca_V1.2$ sparklets, which contributed to regulation of vascular reactivity during angiotensin II signaling.[47–49] Altogether, these data highlight the power of TIRFM in uncovering key mechanistic information in different processes.

5.8 CONCLUDING REMARKS

TIRFM is a powerful technique that has enabled the examination of numerous processes at the membrane/submembrane region with high spatiotemporal resolution. TIRFM has deepened our understanding of submembrane Ca^{2+} signals by facilitating the study of Ca^{2+} microdomains mediated by plasmalemmal Ca^{2+}-permeable channels. Accordingly, the use of TIRFM in combination with conventional electrophysiology has revealed unique features about the organization, function, and regulation of plasmalemmal L-type $Ca_V1.2$ channels and TRPV4 channels in vascular smooth muscle during physiological and pathological conditions. TIRFM can also be used to unmask distinctive elementary Ca^{2+} signals produced by other Ca^{2+}-permeable channels, as well as their trafficking patterns and potentially unique functional modulation by kinases, phosphatases, and signaling molecules in vascular smooth muscle. This will be critical to gain a better appreciation of how these processes shape vascular smooth muscle function and arterial reactivity in physiological and pathological conditions. Finally, it will be important to apply this technique to the study of Ca^{2+}-permeable channels and signaling proteins in native vascular smooth muscle cells from human subjects. This approach may reveal new information about the organization, function, regulation, and trafficking of ion channels and signaling proteins specific to humans.

ACKNOWLEDGMENTS

We thank Dr. Arsalan Syed and Miss Maria Paz Prada for critically reading previous versions of this chapter. This work was supported by National Institutes of Health grants 1R01HL098200, 1R01HL121059, 1R01HL085686, and 1R01HL085870.

REFERENCES

1. Axelrod, D. Selective imaging of surface fluorescence with very high aperture microscope objectives. *J Biomed Opt*. 2001;6:6–13.
2. Axelrod, D, Thompson, NL, Burghardt, TP. Total internal inflection fluorescent microscopy. *J Microsc*. 1983;129 Pt 1:19–28.
3. Nystoriak, MA, Nieves-Cintron, M, Navedo, MF. Capturing single L-type Ca(2+) channel function with optics. *Biochim Biophys Acta*. 2013;1833:1657–1664.
4. Demuro, A, Parker, I. Imaging single-channel calcium microdomains. *Cell Cal*. 2006;40:413–422.
5. Mattheyses, AL, Simon, SM, Rappoport, JZ. Imaging with total internal reflection fluorescence microscopy for the cell biologist. *J Cell Sci*. 2010;123:3621–3628.

6. Fish, KN. Total internal reflection fluorescence (TIRF) microscopy. *Curr Protoc Cytom*. 2009;Chapter 12:Unit12–18.
7. Amberg, GC, Navedo, MF. Calcium dynamics in vascular smooth muscle. *Microcirculation*. 2013;20:281–289.
8. Santana, LF, Navedo, MF. Molecular and biophysical mechanisms of Ca^{2+} sparklets in smooth muscle. *J Mol Cell Cardiol*. 2009;47:436–444.
9. Demuro, A, Parker, I. Imaging the activity and localization of single voltage-gated Ca^{2+} channels by total internal reflection fluorescence microscopy. *Biophys J*. 2004;86:3250–3259.
10. Demuro, A, Parker, I. Optical single-channel recording: Imaging Ca^{2+} flux through individual ion channels with high temporal and spatial resolution. *J Biomed Opt*. 2005;10:11002.
11. Demuro, A, Parker, I. Optical patch-clamping: Single-channel recording by imaging Ca^{2+} flux through individual muscle acetylcholine receptor channels. *J Gen Physiol*. 2005;126:179–192.
12. Mercado, J, Baylie, R, Navedo, MF, Yuan, C, Scott, JD, Nelson, MT, Brayden, JE, Santana, LF. Local control of TRPV4 channels by AKAP150-targeted pkc in arterial smooth muscle. *J Gen Physiol*. 2014;143:559–575.
13. Navedo, MF, Amberg, G, Votaw, SV, Santana, LF. Constitutively active L-type Ca^{2+} channels. *Proc Natl Acad Sci USA*. 2005;102:11112–11117.
14. Navedo, MF, Amberg, GC. Local regulation of L-type Ca(2+) channel sparklets in arterial smooth muscle. *Microcirculation*. 2013;20:290–298.
15. Navedo, MF, Santana, LF. Cav1.2 sparklets in heart and vascular smooth muscle. *J Mol Cell Cardiol*. 2013;58:67–76.
16. Wang, SQ, Song, LS, Lakatta, EG, Cheng, H. Ca^{2+} signalling between single L-type Ca^{2+} channels and ryanodine receptors in heart cells. *Nature*. 2001;410:592–596.
17. Navedo, MF, Amberg, GC, Westenbroek, RE, Sinnegger-Brauns, MJ, Catterall, WA, Striessnig, J, Santana, LF. Cav1.3 channels produce persistent calcium sparklets, but $Ca_v1.2$ channels are responsible for sparklets in mouse arterial smooth muscle. *Am J Physiol Heart Circ Physiol*. 2007;293:H1359–H1370.
18. Sonkusare, SK, Bonev, AD, Ledoux, J, Liedtke, W, Kotlikoff, MI, Heppner, TJ, Hill-Eubanks, DC, Nelson, MT. Elementary Ca^{2+} signals through endothelial TRPV4 channels regulate vascular function. *Science*. 2012;336:597–601.
19. Sullivan, MN, Gonzales, AL, Pires, PW, Bruhl, A, Leo, MD, Li, W, Oulidi, A, et al. Localized TRPA1 channel Ca^{2+} signals stimulated by reactive oxygen species promote cerebral artery dilation. *Sci Signal*. 2015;8:ra2.
20. Zhao, L, Sullivan, MN, Chase, M, Gonzales, AL, Earley, S. Calcineurin/nuclear factor of activated t cells-coupled vanilloid transient receptor potential channel 4 Ca^{2+} sparklets stimulate airway smooth muscle cell proliferation. *Amer J Respir Cell Mol Biol*. 2014;50:1064–1075.
21. Demuro, A, Smith, M, Parker, I. Single-channel Ca(2+) imaging implicates Aβ1-42 amyloid pores in Alzheimer's disease pathology. *J Cell Biol*. 2011;195:515–524.
22. Ullah, G, Demuro, A, Parker, I, Pearson, JE. Analyzing and modeling the kinetics of amyloid beta pores associated with Alzheimer's disease pathology. *PLoS One*. 2015;10:e0137357.
23. Sidaway, P, Teramoto, N. L-type Ca^{2+} channel sparklets revealed by TIRF microscopy in mouse urinary bladder smooth muscle. *PLoS One*. 2014;9:e93803.
24. McCarron, JG, Olson, ML, Currie, S, Wright, AJ, Anderson, KI, Girkin, JM. Elevations of intracellular calcium reflect normal voltage-dependent behavior, and not constitutive activity, of voltage-dependent calcium channels in gastrointestinal and vascular smooth muscle. *J Gen Physiol*. 2009;133:439–457.
25. Zenisek, D, Davila, V, Wan, L, Almers, W. Imaging calcium entry sites and ribbon structures in two presynaptic cells. *J Neurosci*. 2003;23:2538–2548.

26. Navedo, MF, Amberg, GC, Nieves, M, Molkentin, JD, Santana, LF. Mechanisms underlying heterogeneous Ca^{2+} sparklet activity in arterial smooth muscle. *J Gen Physiol*. 2006;127:611–622.
27. Francis, M, Qian, X, Charbel, C, Ledoux, J, Parker, JC, Taylor, MS. Automated region of interest analysis of dynamic Ca(2)+ signals in image sequences. *Am J Physiol Cell Physiol*. 2012;303:C236–C243.
28. Amberg, GC, Navedo, MF, Nieves-Cintrón, M, Molkentin, JD, Santana, LF. Calcium sparklets regulate local and global calcium in murine arterial smooth muscle. *J Physiol*. 2007;579:187–201.
29. Knot, HJ, Nelson, MT. Regulation of arterial diameter and wall [Ca^{2+}] in cerebral arteries of rat by membrane potential and intravascular pressure. *J Physiol*. 1998;508:199–209.
30. Earley, S, Heppner, TJ, Nelson, MT, Brayden, JE. TRPV4 forms a novel Ca^{2+} signaling complex with ryanodine receptors and BKCa channels. *Circ Res*. 2005;97:1270–1279.
31. Zou, H, Lifshitz, LM, Tuft, RA, Fogarty, KE, Singer, JJ. Using total fluorescence increase (signal mass) to determine the Ca^{2+} current underlying localized Ca^{2+} events. *J Gen Physiol*. 2004;124:259–272.
32. Earley, S. Smooth muscle cell Ca(2)(+): Think locally, act globally. *Microcirculation*. 2013;20:279–280.
33. Owsianik, G, Talavera, K, Voets, T, Nilius, B. Permeation and selectivity of TRP channels. *Annu Rev Physiol*. 2006;68:685–717.
34. Dai, S, Hall, DD, Hell, JW. Supramolecular assemblies and localized regulation of voltage-gated ion channels. *Physiol Rev*. 2009;89:411–452.
35. Navedo, MF, Takeda, Y, Nieves-Cintron, M, Molkentin, JD, Santana, LF. Elevated Ca^{2+} sparklet activity during acute hyperglycemia and diabetes in cerebral arterial smooth muscle cells. *Am J Physiol. Cell Physiol*. 2010;298:C211–C220.
36. Nystoriak, MA, Nieves-Cintron, M, Patriarchi, T, Buonarati, OR, Prada, MP, Morotti, S, Grandi, E et al. Ser1928 phosphorylation by PKA stimulates L-type Ca^{2+} channel Cav1.2 and vasoconstriction during acute hyperglycemia and diabetes. *Sci Signal*. 2017;10.
37. Navedo, MF, Cheng, EP, Yuan, C, Votaw, S, Molkentin, JD, Scott, JD, Santana, LF. Increased coupled gating of L-type Ca^{2+} channels during hypertension and Timothy syndrome. *Circul Res*. 2010;106:748–756.
38. Navedo, MF, Nieves-Cintron, M, Amberg, GC, Yuan, C, Votaw, VS, Lederer, WJ, McKnight, GS, Santana, LF. AKAP150 is required for stuttering persistent Ca^{2+} sparklets and angiotensin II-induced hypertension. *Circ Res*. 2008;102:e1–e11.
39. Nieves-Cintron, M, Amberg, GC, Navedo, MF, Molkentin, JD, Santana, LF. The control of Ca^{2+} influx and NFATC3 signaling in arterial smooth muscle during hypertension. *Proc Natl Acad Sci USA*. 2008;105:15623–15628.
40. Dixon, RE, Moreno, CM, Yuan, C, Opitz-Araya, X, Binder MD, Navedo, MF, Santana, LF. Graded $Ca^{(2)(+)}$/calmodulin-dependent coupling of voltage-gated Cav1.2 channels. *eLife*. 2015;4.
41. Dixon, RE, Yuan, C, Cheng, EP, Navedo, M, Santana, LF. Calcium signaling amplification by oligomerization of L-type Cav1.2 channels. *Proc Natl Acad Sci USA*. 2012;109:1749–1754.
42. Chung, SH, Kennedy, RA. Coupled Markov chain model: Characterization of membrane channel currents with multiple conductance sublevels as partially coupled elementary pores. *Math Biosci*. 1996;133:111–137.
43. Cheng, EP, Yuan, C, Navedo, MF, Dixon, RE, Nieves-Cintron, M, Scott, JD, Santana, LF. Restoration of normal L-type Ca^{2+} channel function during Timothy syndrome by ablation of an anchoring protein. *Circul Res*. 2011;109:255–261.
44. Crnich, R, Amberg, GC, Leo, MD, Gonzales, AL, Tamkun, MM, Jaggar, JH, Earley, S. Vasoconstriction resulting from dynamic membrane trafficking of TRPM4 in vascular smooth muscle cells. *Am J Physiol. Cell Physiol*. 2010;299:C682–C694.

45. Ding, Y, Winters, A, Ding, M, Graham, S, Akopova, I, Muallem, S, Wang, Y, et al. Reactive oxygen species-mediated TRPC6 protein activation in vascular myocytes, a mechanism for vasoconstrictor-regulated vascular tone. *J Biol Chem*. 2011;286:31799–31809.
46. Bannister, JP, Adebiyi, A, Zhao, G, Narayanan, D, Thomas, CM, Feng, JY, Jaggar, JH. Smooth muscle cell $\alpha_2\beta$-1 subunits are essential for vasoregulation by Cav1.2 channels. *Circul Res*. 2009;105:948–955.
47. Amberg, GC, Earley, S, Glapa, SA. Local regulation of arterial L-type calcium channels by reactive oxygen species. *Circul Res*. 2010;107:1002–1010.
48. Chaplin, NL, Amberg, GC. Hydrogen peroxide mediates oxidant-dependent stimulation of arterial smooth muscle l-type calcium channels. *Am J Physiol. Cell Physiol*. 2012;302:C1382–C1393.
49. Chaplin, NL, Nieves-Cintron, M, Fresquez, AM, Navedo, MF, Amberg, GC. Arterial smooth muscle mitochondria amplify hydrogen peroxide microdomains functionally coupled to L-type calcium channels. *Circ Res*. 2015;117:1013–1023.